Bioconjugate Chemistry

Article

pubs.acs.org/bc

Endocytosis and Intracellular Dissociation Rates of Human Insulin–Insulin Receptor Complexes by Quantum Dots in Living Cells

Jimena Giudice,[†,‡,∥] Elizabeth A. Jares-Erijman,[‡,⊥] and Federico Coluccio Leskow*[,†,§]

[†]Departamento de Química Biológica, IQUIBICEN-CONICET and [‡]Departamento de Química Orgánica, CIHIDECAR-CONICET, Facultad de Ciencias Exactas y Naturales, Universidad de Buenos Aires, Intendente Güiraldes 2160, Ciudad Universitaria, C1428EGA, Buenos Aires, Argentina

[§]Departamento de Ciencias Básicas, Universidad Nacional de Luján, Buenos Aires, Argentina

Supporting Information

ABSTRACT: Insulin signaling is involved in glucose metabolism, cellular growth, and differentiation. Its function is altered in diabetes and many cancer types. Insulin binding to insulin receptor (IR) triggers diverse signaling pathways. However, signal transduction by IR is not mediated exclusively at the cell surface. Activated ligand–receptor complexes are internalized into endosomes from which the IR recruits adapters acting on substrates that are distinct from those accessible at the membrane. We report the biotinylation of human-recombinant insulin (rhIns) specifically at the position 29 of the B chain. We combined visible fluorescent proteins fused to IR and biotinylated rhIns conjugated with streptavidin–quantum dots to perform extended, quantitative experiments in real time. Modified rhIns bound to the IR and conjugated with the quantum dots was internalized with a rate constant (k) of 0.009 min^{-1}. Dissociation of insulin-IR complex in endocytosed vesicles occurred with k = 0.006 min^{-1}.

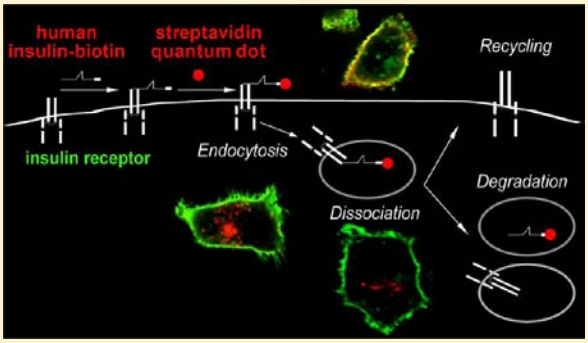

INTRODUCTION

The insulin receptor (IR) is a member of the insulin tyrosine kinase receptor family, which also includes the insulin-like growth factor I (IGF-I) receptor (IGF-IR) and the IR related receptor. The IR can be activated by different ligands leading to different biological effects attributable to differences in receptor interaction, internalization rates, and phosphorylation patterns of the IR and its substrates. Although the major insulin targets are the liver, adipose tissue, and skeletal muscle, IRs are also found in the brain, heart, kidney, pulmonary alveoli, pancreatic acini, placenta vascular endothelium, monocytes, granulocytes, erythrocytes, and fibroblasts.[1] The observation that IRs are not restricted to insulin target tissues suggests that they may be functionally linked to multiple processes in addition to their classical roles in the insulin-dependent regulation of metabolism.

Insulin binding to the IR promotes receptor autophosphorylation and the phosphorylation of IR substrates (IRS-1, IRS-2, and IRS-3), leading to association of IRSs with different effector molecules mediating divergent signaling pathways regulating either glucose homeostasis and metabolic gene expression or cell growth and differentiation.[1,2] The metabolic effect of insulin is mediated by recruitment and activation of Akt at the cell membrane, leading to the translocation of the glucose transporter 4 (GLUT4) promoting the uptake of glucose and fatty acids, and synthesis of glycogen and protein. Insulin also activates the cascade that leads to activation of mitogen-activated protein kinase (MAPK) and mitogenic responses including gene transcription stimulated by FOS and ELK1.[3] This last pathway operates independently of IRS, acting via the interaction of IR with the adaptor protein SHC that associates with GRB2 and thus engages the activation sequence for RAS and MAPK.[4−7]

Signal transduction by IR is not limited to its activation at the cell surface. The activated ligand–receptor complex is internalized into endosomes, and this process is dependent on kinase autophosphorylation.[8] Endocytosis of activated receptors has the dual effect of concentrating receptors within endosomes and allowing the IR tyrosine kinase to phosphorylate substrates spatially distinct from those accessible at the plasma membrane.[9−15] Acidification of the endosomal lumen results in dissociation of insulin from its receptor and signaling termination. Receptors could be recycled to the plasma membrane or transported to lysosomes for degradation. The lifetime of a ligand–receptor complex within the endosomes impacts the response produced by a particular receptor. Insulin, which has a relatively short endosomal residence, elicits primarily acute metabolic effects, whereas the epidermal growth factor (EGF) and the IGF-I, which have longer endosomal residence times, elicit mitogenic responses.[3] These differences in biological responses probably reflect distinct actions of intracellular signaling molecules at specific cellular locations. Thus,

Received: September 19, 2012
Revised: January 25, 2013
Published: January 29, 2013

dx.doi.org/10.1021/bc300526d | *Bioconjugate Chem.* 2013, 24, 431−442

differences in ligand residency, along with differences in the intrinsic activity of receptors, may contribute to the activation of different signaling pathways.[3]

During the past 30 years, many reports have studied internalization of different receptor−ligand complexes (in particular, insulin−IR) mostly using radioactive ligands in order to measure endocytosis kinetics. These biochemical approaches gave a deep view of cell traffic as an average of cell populations. However, very little was done in order to study insulin−IR complexes endocytosis and dissociation in vivo and in individual cells. In addition, almost all the available data of internalization rates comes from experiments performed with hormones from animal origin (bovine, porcine, etc.).

During the past decade, diverse labeling strategies have provided a spatiotemporal view of the dynamics of proteins in living cells.[16−18] The combination of the visible fluorescent proteins (VFPs) fused to the molecules of interest and quantum dots (QDs) bound to different ligands allowed the study in living cells of the multiple stages of signaling by fluorescence microscopy. QDs provide unique advantages for cellular imaging: (i) intense and uniform brilliance, permitting detection down to the single nanoparticle level, and reliable quantification of binding and transport phenomena; (ii) photostability, allowing imaging over prolonged periods; (iii) broad excitation spectra, allowing the simultaneous excitation of VFPs and QDs; (iv) narrow, tunable emission bands conveniently red-shifted to the fluorescence of the VFPs; (v) biochemical stability and specificity with low background and adjustable stoichiometry (ligands/QDs) afforded by the biotin−streptavidin titration; (vi) ligand compliance, the noninterference of the QD with the biochemical specificity of an attached ligand; and (vi) steric compatibility, as, for example, the ability of two QD-ligands to bind to two monomers of a dimeric receptor.[19]

Biotinylated ligands in combination with streptavidin-conjugated QDs provide valuable tools for studying receptor tyrosine kinase dynamics in living cells, including the characterization of endocytosis and retrograde transport.[19−25] Recently, it was demonstrated that QDs specifically targeted to EGFR can clearly distinguish low-grade as well as high-grade glioma tissue from normal brain tissue both at the macroscopic and the single cell level with high contrast ratios. The strong and photostable fluorescence and rapid differential binding of these probes meet some of the criteria required by surgeons to distinguish tumor cells left in the resection cavity.[26]

Here, we addressed the study of IR internalization using the advantages of the QD to track the endocytosis of ligand−receptor complexes in individual cells. We modified human recombinant insulin (rhIns) by introducing a biotin group specifically in the lysine located at the position 29 of the B chain (B_{29}). We incorporated a linker of ∼18 Å in order to maintain biological activity and increase accessibility. The modification allowed subsequent conjugation with streptavidin−QDs and thus the visualization of human insulin binding specifically to the IR-B fused to the super yellow fluorescent protein (SYFP) in vivo. We imaged endocytosis and trafficking of the human insulin-QD655-IR-SYFP complex in real time, performing quantitative assessment of ligand−receptor internalization and colocalization. These procedures led to the estimations of the rate constants and lifetime of the internalized insulin-IR complexes.

EXPERIMENTAL PROCEDURES

Materials. rhIns was kindly provided by Laboratorios Beta (Argentina). The streptavidin-QD655 was from Molecular Probes (# Q10121MP), Invitrogen (Eugene, OR). Bovine insulin conjugated with FITC (FITC-Ins) and biotin amido caproyl insulin (BAC-Ins) were from SIGMA (Saint Louis, MO). Lipofectamine Reagent 2000 was from Invitrogen (Carlsbad, CA). Dialysis membrane (<3500 Da) was from Cellu Sep (Seguin, TX). Mouse monoclonal antihuman influenza hemagglutinin (HA) was from Covance (Emeryville, CA). Mouse monoclonal anti-PY99, rabbit polyclonal antiphosphorylated Akt (Ser 473), and rabbit polyclonal anti-ERK2 were from Santa Cruz Biotechnology (Santa Cruz, CA). Mouse monoclonal anti-IR-β-subunit, rabbit monoclonal anti-p-Akt (Ser 473, immunofluorescence experiments), and rabbit monoclonal anti-p-MAPK (p44/42) were from Cell Signaling Technology (Danvers, MA). For specific IR phosphorylation detection, we used rabbit monoclonal anti-p-IR-β subunit (Tyr 1361) from Cell Signaling (cat #3023) which detects transfected levels of IR β subunit and only slightly cross-reacts with IGF-I receptor.

Plasmid Generation. *pcDNA3-IR-B:* cDNA of IR-B was provided by Dr. A. Ullrich (Max Planck Institute for Biophysical Chemistry, Germany) and amplified by PCR using primers containing *Hin*dIII restriction site (IR-Forward: 5′-aagcttatggcca-ccgggggccgg-3′) and NheI and XbaI sites (IR-Reverse: 5′-tctagagc-tagcgaaggattggaccgaggcaaggtc-3′). The product was digested with *Hin*dIII and XbaI enzymes and cloned into pcDNA3 vector. *pcDNA3-IR-B-GFP, pcDNA3-IR-B-SCFP and pcDNA3-IR-B-SYFP:* peGFP-C3 (Clontech), pSCFP-3AC, or pSYFP-2F (provided by T. W. Gadella Jr., University of Amsterdam, The Netherlands) were digested with NheI and ApaI, and cloned into pcDNA3-IR-B.

Chemical Modification of rhIns. The rhIns was biotinylated in a two-step synthesis: first, by generation of *N*-hydroxysuccinimide (NHS) ester of biotin bound to 4 poly(ethylene oxide) (PEO) groups (PEO_4-biotin) from the corresponding acid. One equivalent (equiv) (0.0042 mmol) PEO_4-biotin acid was reacted with 2 equiv NHS in dimethylformamide (DMF); 2.5 equiv of *N,N*′-dicyclohexilcarbodiimide (DCC) was added, and after reaction for 4 h at room temperature (RT), the products were monitored by TLC in reverse-phase (methanol−water (3:1 and 1:2) as mobile phase). We modified the conditions reported by Jensen and Wilkinson[27] in order to covalently bind the PEO_4-biotin to rhIns. The product of the first step was mixed with 0.0045 mmol rhIns dissolved in DMF/triethylamine (TEA) during 6 h at RT. The reaction was monitored by TLC in reverse phase (methanol−water (3:1) as mobile phase). The reaction was stopped by adding 1 M acetic acid, dialyzed against milliQ water for 3 days (renewed every 12 h), lyophilized, and analyzed by matrix-assisted laser desorption/ionization (MALDI-TOF) (Ultraflex II, Bruker, CEQUIBIEM, FCEN, UBA, Argentina): (i) without any treatment; (ii) after treatment with 20 mM DTT and 100 mM iodoacetamide for 15 min at RT; (iii) after treatment with trypsin for 1−2 h at 37 °C; and (iv) after treatment with trypsin and subsequently with dithiothreitol (DTT).[28] For MALDI characterization, the solid sample was dissolved in 2 M urea, 15 mM Tris-HCl pH 8.0, and diluted in 50 mM $(NH)_4HCO_3$. Sinapinic acid (10 mg/mL) dissolved in 70% acetonitrile/0.125% TFA was used as matrix.

Cell Culture and Transfection. Cell culture reagents (Dulbecco's modified Eagle's medium (DMEM) Glutamax, Optimem, fetal bovine serum (FBS), trypsin, supplements, and

dx.doi.org/10.1021/bc300526d | *Bioconjugate Chem.* 2013, 24, 431−442

antibiotics) were from GIBCO (Grand Island, NE). HeLa, CHO, and Cos cells (ATCC-CCL-2) were maintained in DMEN supplemented with penicillin, streptomycin, and 10% (v/v) FBS at 37 °C in 5% CO_2. HEK 293 cells were maintained similarly but supplemented with 1 mM sodium pyruvate. For HepG2 cells, we used a nonessential amino acid supplement (0.1 mM). Cells were plated at 1×10^5 cells/well in 24 well plates onto 12 mm glass coverslips one day before transfection in DMEM/10% (v/v) FBS without antibiotics. Cells were transfected with Lipofectamine Reagent 2000 for 5 h (0.4 μg DNA and 1 μL Lipofectamine per well in DMEM no adds). After transfection, cells were cultured for 12 h in DMEM/10% (v/v) FBS and then for 48 h in DMEM/10% (v/v) FBS/streptomycin and penicillin.

Western Blots. Following stimulation with 100 nM rhIns or FITC-Ins 10 min, cells were lysed in buffer containing 50 mM Tris-HCl pH 7.5, 1 mM EDTA, 1 mM EGTA, 150 mM NaCl, 10% (v/v) glycerol, 1% (v/v) NP40, 1 mM $MgCl_2$, 0.1% (v/v) SDS, 2 mM Na_3VO_4, 40 mM sodium β-glycerophosphate, 1 mM DTT, 1 mM NaF, and a protease inhibitor cocktail (Roche), centrifuging for 10 min at 13 000*g* at 4 °C. Supernatants were mixed with loading buffer (50 mM Tris-HCl pH 6.8, 2% (v/v) SDS, 0.1% (w/v) Bromophenol blue, 10% (v/v) glycerol, 100 mM β-mercaptoethanol) and heated for 5 min at 100 °C. Following 10% SDS-PAGE and transfer, membranes were blocked in 5% (w/v) nonfat dried milk in 0.1% (v/v) Tween-TBS buffer (TTBS) for 1 h, washed and incubated overnight at 4 °C with primary antibodies diluted in 5% (w/v) BSA/TTBS (anti-IR-β-subunit, 1/500; anti-ERK2, 0.4 μg/mL; anti-p44/42 MAPK, 1/500; anti-p-Akt, 0.4 μg/mL; anti-HA, 1/1000) or in 2% (w/v) BSA/TTBS (anti-PY20, 2 μg/mL). The following day, membranes were incubated with secondary antibodies for 1 h and washed. Blots were developed by chemiluminescence using a Bio-Imaging Analyzer Bas-1800II and Image Gauge 3.12, FUJIFILM (FCEN, UBA. Argentina).

FITC-Ins Labeling. Before the experiment, cells expressing IR-B, starved overnight, were washed with Tyrode's buffer (135 mM NaCl, 10 mM KCl, 10 mM $MgCl_2$, 1 mM $CaCl_2$, 10 mM HEPES pH 7.2, 0.1% (w/v) BSA) at RT and incubated with 50 nM FITC-Ins for 15 min at 15 °C. Cells were either fixed in 3.7% PFA on ice during 20 min or incubated at 37 °C for different periods of time before fixation.

Labeling in Vivo with QDs and Biotinylated Insulins and Internalization. Before the experiment, cells expressing IR-B or IR-B-VFP were starved overnight, washed with Tyrode's buffer, and labeled following a two-step protocol by incubating with 50 nM FITC-Ins or 50 nM BAC-Ins or rhIns-PEO_4-biotin for 15 min, washing with Tyrode's buffer, and subsequently incubating with 1 nM QD655 for 10 min in darkness. After washing, cells were incubated at 37 °C in DMEM for different time periods before fixation or live visualization.

Immunofluorescence. After overnight starvation, transfected cells were stimulated with 100 nM rhIns, FITC-Ins, or BAC-Ins for 10 min, washed with PBS, and immediately fixed in cold methanol for 30 min at −20 °C, blocked with PBS/0.3% (v/v) Triton X-100/1% (w/v) BSA for 1 h at 37 °C and incubated with anti-PY99 (1 μg/mL), anti-p-Akt (Ser 473; Cell Signaling, 1/200), or anti-p-IR β subunit (0.3 μg/mL) overnight at 4 °C. The following day, samples were incubated with a secondary antibody conjugated with Cy3 during 1 h at 37 °C and washed.

Microscopy. Confocal laser scanning microscopy was performed with the following microscopes: (i) Olympus Fluoview FV 1000 with a UPLSAPO 60× 1.2 NA water immersion objective. Excitation and emission filters were as follows: excitation SYFP, 515 nm; emission SYFP, band-pass (BP) 535−565 nm; excitation QD655, 405 nm; emission QD655, BP 585−685 nm. (ii) Zeiss LSM 510 Meta with a Plan-Apochromat 63× 1.4 NA oil immersion objective. Excitation and emission filters were as follows: excitation FITC, 488 nm; emission FITC, 510−563 nm; excitation Cy3, 532 nm; emission Cy3, 563−606 nm; excitation GFP, 488 nm, emission GFP, BP 500/20 nm; excitation QD655, 488 and 458 nm; emission QD655, LP 650 nm.

Wide-field microscopy was carried out with an Olympus IX71 microscope with a 40× 1.15 NA water-immersion objective or a Zeiss Axiovert S100 with a 63× 1.25 NA oil immersion objective (Zeiss). A mercury arc lamp excitation and suitable filter were used. Camera: Hamamatsu Orca CCD C4742−95.

Image Processing. Images were processed with *Matlab* (TU Delft, The Netherlands, http://www.ph.tn.tudelft.nl/DIPlib/index.html) and *ImageJ* (http://rsb.info.nih.gov, NIH). Background of each channel (mean of empty region for *ImageJ* and image median for *Matlab*) was subtracted and, in some cases, a median filter was applied (radius: 1 pixel) only for presentation. For wide field experiments (Akt activation), *z*-stacks (80 frames, 0.2 μm step size) were deconvolved using *Huygens Professional Scientific Volume Imaging* v 3.6 software, applying a quick maximum likelihood estimation algorithm.

Internalization Analysis. For quantitative internalization experiments, we defined the onset time as the end of labeling washes, and cells were incubated at 37 °C for 20, 40, 35, 95, 150, 160, and 300 min of incubation at 37 °C.

Segmentation (Cell and Interior). Channel backgrounds were subtracted. Segmentation was performed for each cell using VFP signal or DIC image. After cell and interior segmentation, we measured QD655 signal in both regions with *ImageJ* or *Matlab*.

Estimation of the Internalization Ratio. To compute the relative amount of internalized fluorescence, we estimated QD_{total} as the measurements of the QD655 in the region cell and the $QD_{interior}$ as the measurements in the region interior. Finally, we calculated for each cell the ratio $QD_{interior}/QD_{total}$. This "internal calibration" approach was chosen to remove influence of amplifier gain and zoom factor for each image acquisition condition.

Colocalization Analysis. Manders coefficient and PDM (differences from the mean) and frequencies plots were performed with *ImageJ* plugin "Intensity correlation analysis". Manders coefficients were calculated by eqs 1−3.

$$M = \frac{\sum (\mathrm{Im}_{\mathrm{syfp}} \times \mathrm{Im}_{\mathrm{QD655}})}{\sqrt{\sum (\mathrm{Im}_{\mathrm{syfp}})^2 \times \sum (\mathrm{Im}_{\mathrm{QD655}})^2}} \quad (1)$$

$$M_{\mathrm{syfp}} = \frac{\sum_i \mathrm{Im}_{\mathrm{syfpicoloc}}}{\sum_i \mathrm{Im}_{\mathrm{syfpi}}} \quad (2)$$

$$M_{\mathrm{QD655}} = \frac{\sum_i \mathrm{Im}_{\mathrm{QD655icoloc}}}{\sum_i \mathrm{Im}_{\mathrm{QD655}}} \quad (3)$$

where Im_{syfp} = image from SYFP channel; Im_{QD655} = image from QD655 channel; $Im_{syfpicoloc}$ and $Im_{qd655icoloc}$ = colocalized pixels in Im_{syfp} and Im_{qd655}.

For each pixel, PDM value was calculated by eq 4:

$$\mathrm{PDM} = (\mathrm{Im}_{\mathrm{yfp}} - \overline{\mathrm{Im}_{\mathrm{syfp}}}) \times (\mathrm{Im}_{\mathrm{QD655}} - \overline{\mathrm{Im}_{\mathrm{QD655}}}) \quad (4)$$

We used the loss of colocalization degree as an estimation of the dissociation between ligand and receptor. High colocalization

dx.doi.org/10.1021/bc300526d | *Bioconjugate Chem.* 2013, 24, 431−442

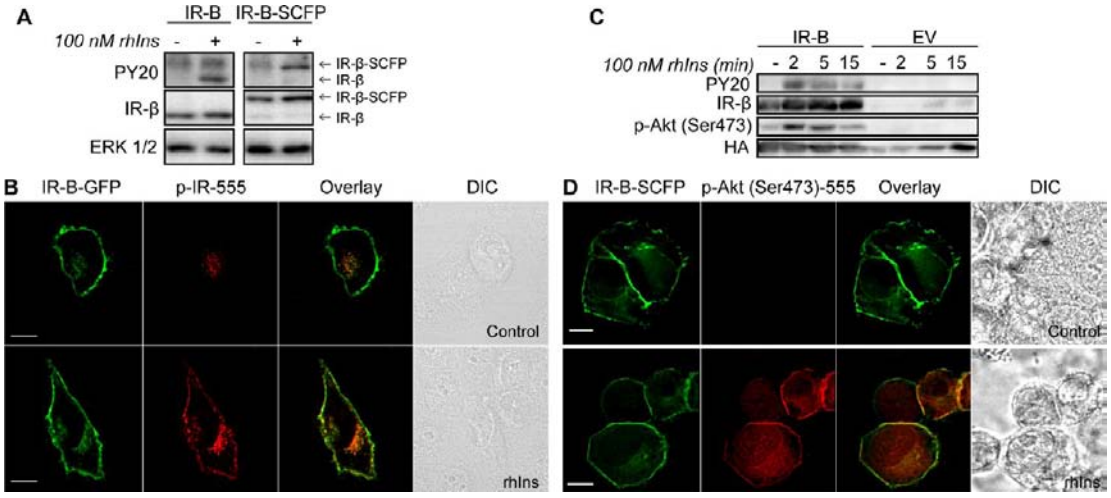

Figure 1. Expression and function of IR-B chimeras. A. HeLa cells expressing IR-B or IR-B-SCFP were starved overnight in DMEM/0.1% BSA. Then, cells were stimulated with 100 nM rhIns for 10 min and lysates were assayed by Western blot. B. HeLa cells expressing IR-B-GFP were treated in the same way, but they were assayed by immunofluorescence using a specific primary antibody against p-IR and a secondary antibody conjugated with Alexa Fluor 555. Imaging was carried out by confocal microscopy (Zeiss LSM 510 Meta). Scale bars: 10 μm. C. Akt phosphorylation (Ser473) profile in cells coexpressing Akt-HA and IR-B or EV, starved for 16 h, and stimulated with 100 nM rhIns for 2, 5, and 15 min. D. Immunofluorescence experiments by wide-field microscopy (Olympus IX71) showing Akt phosphorylation in response to insulin. Deconvolved middle frame of 80 z-stacks with 0.2 μm step size. Scale bars: 10 μm.

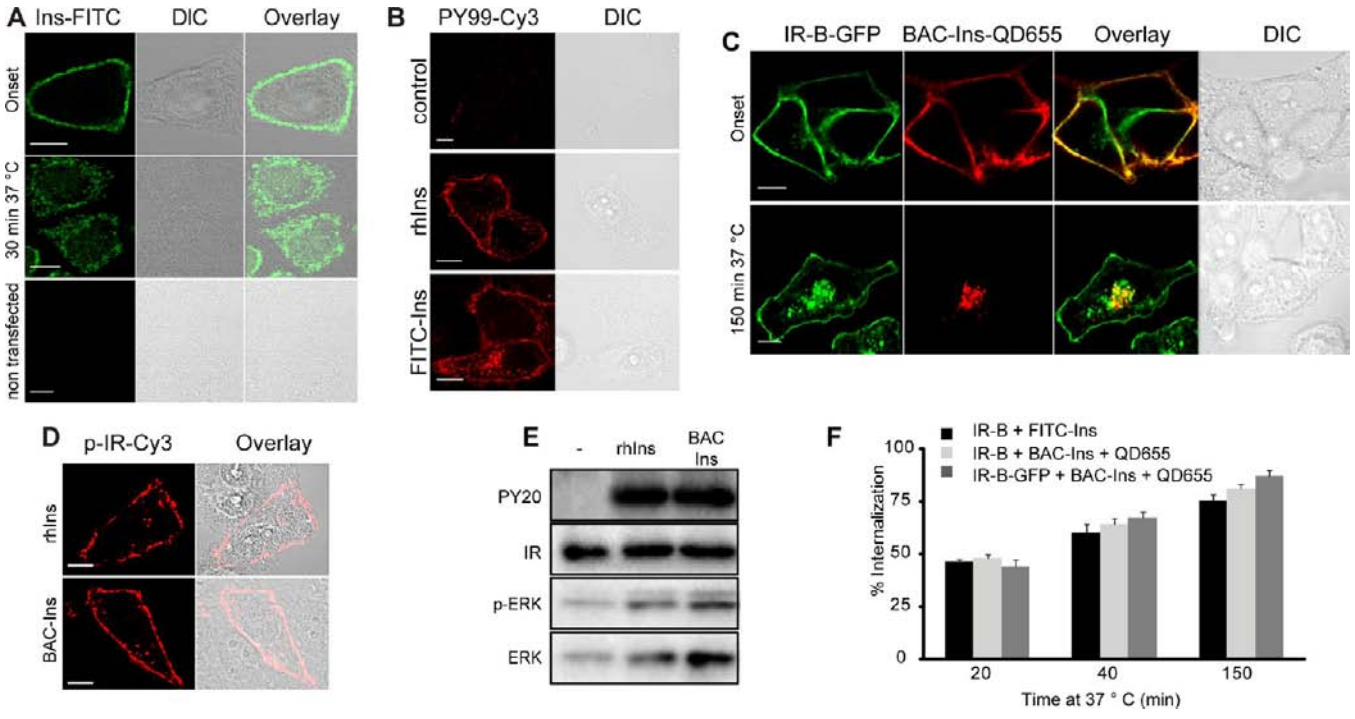

Figure 2. Fluorescent and biotinylated insulins in combination with QD. A. HeLa cells expressing IR-B were starved overnight and then labeled with 50 nM FITC-Ins for 15 min at 15 °C. Cells were fixed directly or after incubation at 37 °C for 30 min. B. HeLa cells expressing IR-B were starved for 18 h, stimulated with 50 nM FITC-Ins or rhIns for 10 min. After fixation, samples were assayed by immunofluorescence using an anti-p-Tyr (PY99) and a secondary antibody conjugated with Cy3. C. HeLa cells expressing IR-B-GFP were starved overnight and sequentially incubated for 10 min at 15 °C with 50 nM BAC-Ins followed by 1 nM QD655 and fixed (upper panel) or incubated at 37 °C for 150 min prior to fixation (lower panel). D,E. HeLa cells expressing IR-B were starved overnight and stimulated with 100 nM rhIns for 10 min. Samples were assayed by immunofluorescense (anti-p-Tyr (PY99); panel D) or by Western blot (anti-p-Tyr (PY20), IR β-subunit, p-ERK 1/2 and total ERK; panel E). Imaging was performed by confocal microscopy (Zeiss LSM 510 Meta). Scale bars: 10 μm. F. Cell-by-cell quantification of internalized IR-B-Insulin complexes was performed using *Matlab*. The same analysis was performed for IR-B-FITC-Ins, IR-B-BAC-Ins-QD655, and IR-B-GFP-BAC-Ins-QD655 complexes. Results are shown as the mean ± s.e.m. (n = 9−39 cells.)

coefficient means ligand−receptor association; low coefficients means lower association.

Statistical Analysis. Results were expressed as the mean of at least 3 independent experiments ± s.e.m. p values were estimated using two-tailed Student's t tests.

Graphical Fitting. Curves for internalization rates and colocalization data were fitted by *Origin 8.6*. For internalization data, we used a Sigmoidea logistic curve, and for colocalization, we applied a dose response model for fitting. In both cases, R^2 = 0.99 allowing us to conclude that fitting was appropriate.

dx.doi.org/10.1021/bc300526d | *Bioconjugate Chem.* 2013, 24, 431−442

Table 1. Internalization of Bovine Insulin-IR Complexes[a]

	IR-B + FITC-Ins			IR-B + BAC-Ins + QD			IR-B-GFP + BAC-Ins + QD		
time (min)	av (%)	s.e.m. (%)	*n* (cells)	av (%)	s.e.m. (%)	*n* (cells)	av (%)	s.e.m. (%)	*n* (cells)
20	46	1	12	48	2	17	44	3	21
40	60	4	12	64	3	39	67	3	22
150	75	3	15	81	2	23	87	3	9

[a]Cell-by-cell quantification of internalized IR-Insulin complexes was performed using *Matlab*. The same analysis was performed for IR-B-FITC-Ins, IR-B-BAC-Ins-QD655, and IR-B-GFP-BAC-Ins-QD655 complexes.

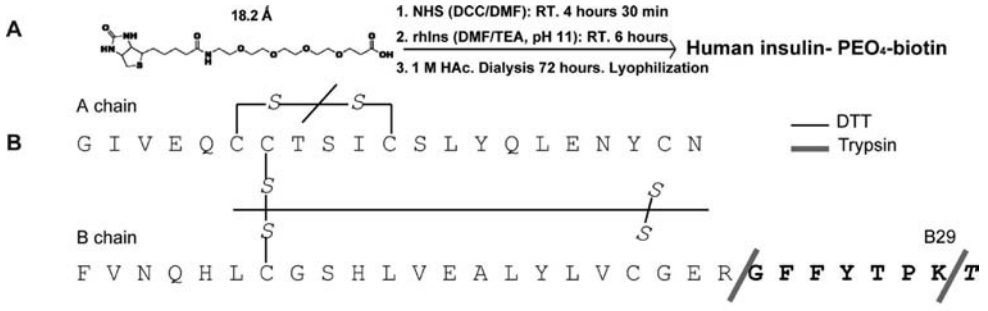

C

	Sequence	Mass (Da)
A chain	GIVEQCCTSICSLYQLENYCN	2383.0
B chain	FVNQHLCGSHLVEALYLVCGER**GFFYTPK*T***	3428.7
Dipeptide-6 Hidrogen (from disulfide bonds)	GIVEQCCTSICSLYQLENYCN + FVNQHLCGSHLVEALYLVCGER**GFFYTPK*T*** − 6 Hidrogen	5805.7
Peptide result from trypsin digestion	**GFFYTPK** and ***T*** or **GFFYTPK*T***	859.4 and 120.1 or 979.0
Insulin without **GFFYTPK**	GIVEQCCTSICSLYQLENYCN + FVNQHLCGSHLVEALYLVCGER	4826.2
Insulin without last ***T***	GIVEQCCTSICSLYQLENYCN + FVNQHLCGSHLVEALYLVCGER**GFFYTPK**	5685.6

Figure 3. Modification of rhIns and fragmentation analysis. A. Biotinylation of rhIns. B. Amino acid sequence of human insulin and scheme of the consequences of different treatments used for MALDI-TOF characterization. S−S indicates disulfide bonds. C. The table shows the mass (Da) for A and B chains of rhIns, the dipeptide with the disulfide bonds, and the peptides obtained after trypsin treatment.

Therefore, we calculated the first derivative as a measurement of the rate of internalization or dissociation (k). The maximum ligand−receptor internalization or dissociation rates were obtained by determining the zero of the second derivate of the curve.

RESULTS

Generation and Expression of IR-B Chimeras. We generated vectors expressing IR-B wild-type or fused with the visible fluorescent proteins green (eGFP), cyan (SCFP-3AC), and yellow (SYFP-2F). Different human cell lines (HeLa, HEK 293, HepG2) were transfected with these plasmids showing correct localization of IR-B at the plasma membrane. However, nonhuman cells (CHO y Cos7) showed protein accumulation at the Golgi probably due to failures in protein folding and post-translational modifications (Figure S1). We decided to continue our experiments in HeLa cells given their low levels of endogenous IR and their morphology and reduced autofluorescence.

It is known that, after insulin binding, IR changes its conformation and is autophosphorylated in different residues of its kinase domain. These events lead to Akt pathway activation regulating different cellular processes such as glucose metabolism, growth, gene expression, and differentiation. We evaluated IR phosphorylation either by Western blot (with a generic antibody against p-Tyr, PY20) or by immunofluorescence using a specific antibody against the phosphorylated IR-β subunit (Figure 1A,B). Both approaches confirmed specific activation of the chimeras since nontransfected cells did not show phosphorylation signal. Activation signal was majorly localized at the plasma membrane at 10 min; however, some endocytosed signal is detected close to the membrane coming from activated IRs inside the endosomes (Figure 1B). We evaluated Akt activation (phosphorylation of Ser 473) in cells expressing IR-B or IR-B-SCFP and Akt-HA. We performed these experiments by Western blot (Figure 1C) and immunofluorescence (Figure 1D). Both approaches confirmed that IR-B and IR-B-VFP were able to activate Akt signaling in response to rhIns.

Visualization of Internalized IR-B with FITC-Ins and BAC-Ins-QD655. Commercially available FITC-Ins bound to the receptor in cells overexpressing IR-B (Figure 2A). Immunofluorescence using an antibody against phosphorylated Tyr (PY99) showed autophosphorylation in transfected cells, whereas nontransfected cells did not show any signal (Figure 2B). To assess the internalization of the insulin-IR complexes, cells were incubated at 37 °C for 30 min after stimulation with FITC-Ins. We confirmed FITC-ins-IR internalization (Figure 2A), although we discovered numerous

dx.doi.org/10.1021/bc300526d | *Bioconjugate Chem.* 2013, 24, 431−442

Table 2. Predicted Molecular Masses[a]

	Compound	No treatment	DTT A chain	DTT B Chain	Triypsin	Trypsin + DTT
A_1	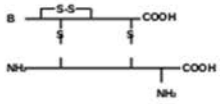	6278.9	2856.2	3428.7	5299.9 979.0 859.4	2856.2 2449.7 979.0 859.4
B_1	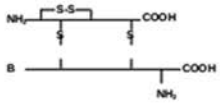	6278.9	2383.0	3901.9	5299.9 979.0 859.4	2383.0 2922.9 979.0 859.4
B_{29}	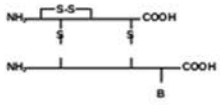	6278.9	2383.0	3901.9	4826.7 1452.2 1332.6	2383.0 2449.7 1452.2 1332.6
A_1B_1	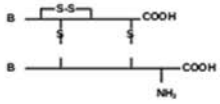	6752.1	2856.2	3901.9	5773.1 979.0 859.4	2856.2 2922.9 979.0 859.4
A_1B_{29}	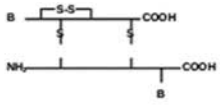	6752.1	2856.2	3901.9	5299.9 1452.2 1332.6	2856.2 2449.7 1452.2 1332.6
B_1B_{29}	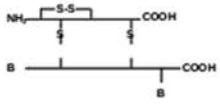	6752.1	2383.0	4375.1	5299.9 1452.2 1332.6	2383.0 2922.9 1452.2 1332.6
$A_1B_1B_{29}$	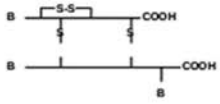	7225.4	2856.2	4375.1	5773.1 1452.2 1332.6	2856.2 2922.9 1452.2 1332.6
Insulin	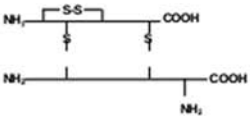	5805.7	2383.0	3428.7	4826.7 979.0 859.4	2383.0 2449.7 979.0 859.4

[a]Predicted molecular masses (Da) are shown for each treatment (DTT, trypsin, and trypsin + DTT) of insulin, mono-biotinylated insulin (A1, B1, and B29), di-biotinylated insulin (A1B1, A1B29, and B1B29), and tri-biotinylated insulin (A1B1B29). B indicates PEO_4-biotin.

disadvantages: FITC-Ins background signal, fluorophore stability is low, and, most important, its fluorescence is affected by the low pH of the endosomes. This scenario led us to design a strategy taking advantage of commercially available streptavidin conjugated QD in combination with biotinylated human recombinant insulin. To verify whether the conjugation of the ligand with nanoparticles of ~20 nm or fusion with VFPs of the receptor affects endocytosis dynamics, we used commercially available bovine insulin (BAC-Ins). HeLa cells expressing IR-B-GFP were treated with 50 nM BAC-Ins and after washes subsequently labeled with streptavidin QD655. Cells were directly fixed or previously incubated at 37 °C for 150 min. Labeling was specific: nontransfected cells did not show QD655 signal (Figure 2C). Additionally, internalization was not affected, since after 150 min, almost all the QD655 signal was detected intracellularly. We confirmed by Western blot and immunofluorescence that ligand biotinylation does not affect the biological activity: BAC-Ins triggered IR-B and ERK 1/2 phosphorylation at similar levels that rhIns (Figure 2D,E).

To evaluate if VFP size (~27 kD) or QD size (~18 nm) affects internalization rate, we quantified endocytosis in a cell by cell analysis. Cells were incubated at 37 °C after labeling (either with FITC-Ins or with BAC-Ins+QD655) for 20, 40, or 150 min, fixed on ice, and imaged by confocal microscopy. Using *Matlab* routines, each cell was segmentated into "membrane" and "interior". Intensity of red signal was quantified in both areas, and we estimated the ratio $QD_{membrane}/QD_{membrane+interior}$. These results are shown in Figure 2F and suggest that internalization is not affected by the VFP or by the QD size (Table 1).

dx.doi.org/10.1021/bc300526d | *Bioconjugate Chem.* 2013, 24, 431−442

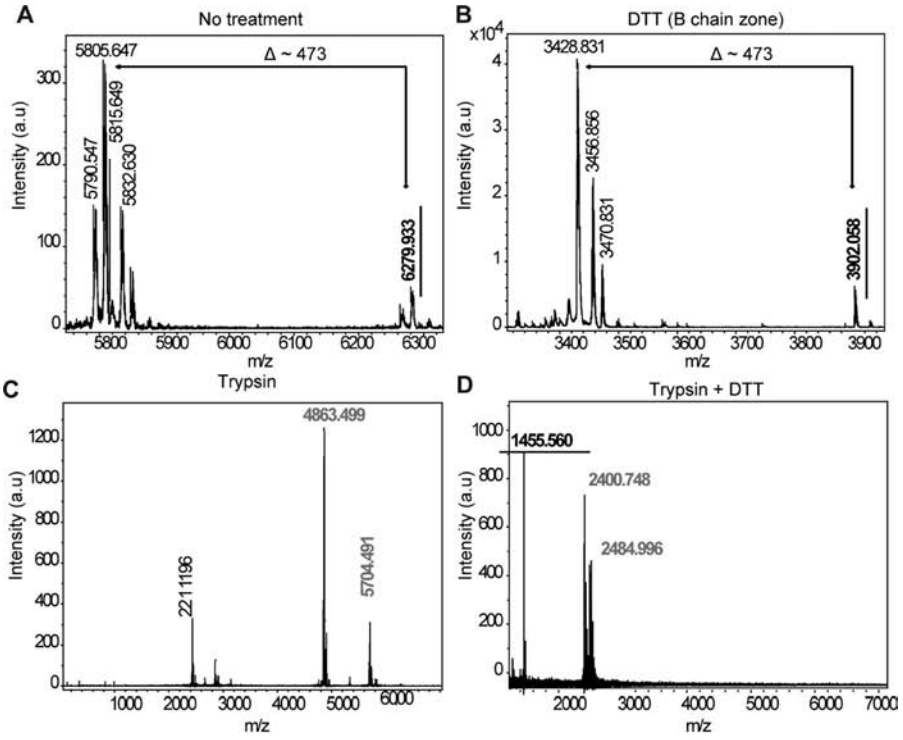

E

Treatment	Experimental peaks (Da)	Predicted molecular mass (Da) for B29 and insulin	Assignment
-	5805.6	5805.7	Insulin
-	**6279.9**	6278.9	A_1, B_1, **B_{29}**
DTT (A chain)	2405.0 2383.0	2383.0 + 23 2383.0	Insulin and/or **B_{29}**, B_1B_{29}
DTT (B chain)	3428.8	3428.7	Insulin
	3902.1	3901.9	B_1, **B_{29}**, A_1B_{29}, B_1B_{29}
Trypsin	4863.5 5704.5	4826.7 + 23 5686.1 + 23	Insulin and/or **B_{29}**
Trypsin + DTT	881.4	859.4 + 23	Insulin
	1455.6	1452.2	**B_{29}**, A_1B_{29}, B_1B_{29}, $A_1B_1B_{29}$
	2400.8 2485.0	2383.0 + 23 2449.7 + 23	Insulin and/or **B_{29}**, A_1B_{29}, B_1B_{29}, $A_1B_1B_{29}$

Figure 4. Characterization of the reaction product by MALDI-TOF. A–D. MALDI-TOF (positive mode) of the reaction product: without treatment (A), after DTT reduction and carbamidomethylation (B), after trypsin treatment for 1–2 h at 37 °C (C) or after treatment with trypsin for 1–2 h at 37 °C and subsequently with 20 mM DTT and 100 mM iodoacetamide for 15 min at RT) (D). The matrix used was sinapinic acid (10 mg/mL) dissolved in 70% acetonitrile, 0.125% TFA. E. Experimental peaks (Da) obtained for the reaction product treated with DTT, trypsin, or both. In bold and underscore, we show the predicted peaks which are exclusively present when B29 residue was modified, and in gray, the ones which are shared with the unmodified insulin molecule. We show predicted molecular masses, experimental peaks, and assignment.

Chemical Modification of rhIns. We generated rhIns covalently bound to biotin through a linker of PEO_4 with a length of ~18 Å. The linker was introduced in order to separate the active part of the hormone from the modified portion of the molecule and minimize interference with insulin function. The synthesis was performed in two steps: (i) generation of NHS ester of PEO_4-biotin; and (ii) reaction between the previous product and rhIns (Figure 3A).

Characterization of reaction products was performed by MALDI-TOF after different treatments: (i) the sample without treatment; (ii) treatment with DTT plus alkylation with iodoacetamide (A and B chains of insulin were obtained after the reduction of disulfide bonds); (iii) treatment with trypsin (this enzyme cleaves after the last Arg located at the position 22 of the B chain (B_{22}) and in some cases can digest after Lys 29 of B chain (B_{29})); or (iv) treatment with trypsin and subsequently with DTT plus iodoacetamide. Figure 3B shows schematically the consequences of each treatment on insulin molecule and Figure 3C summarizes predicted molecular mass for the products of each treatment. Taking this into account and considering the mass of each PEO_4-biotin group (473.2 Da)),

dx.doi.org/10.1021/bc300526d | Bioconjugate Chem. 2013, 24, 431–442

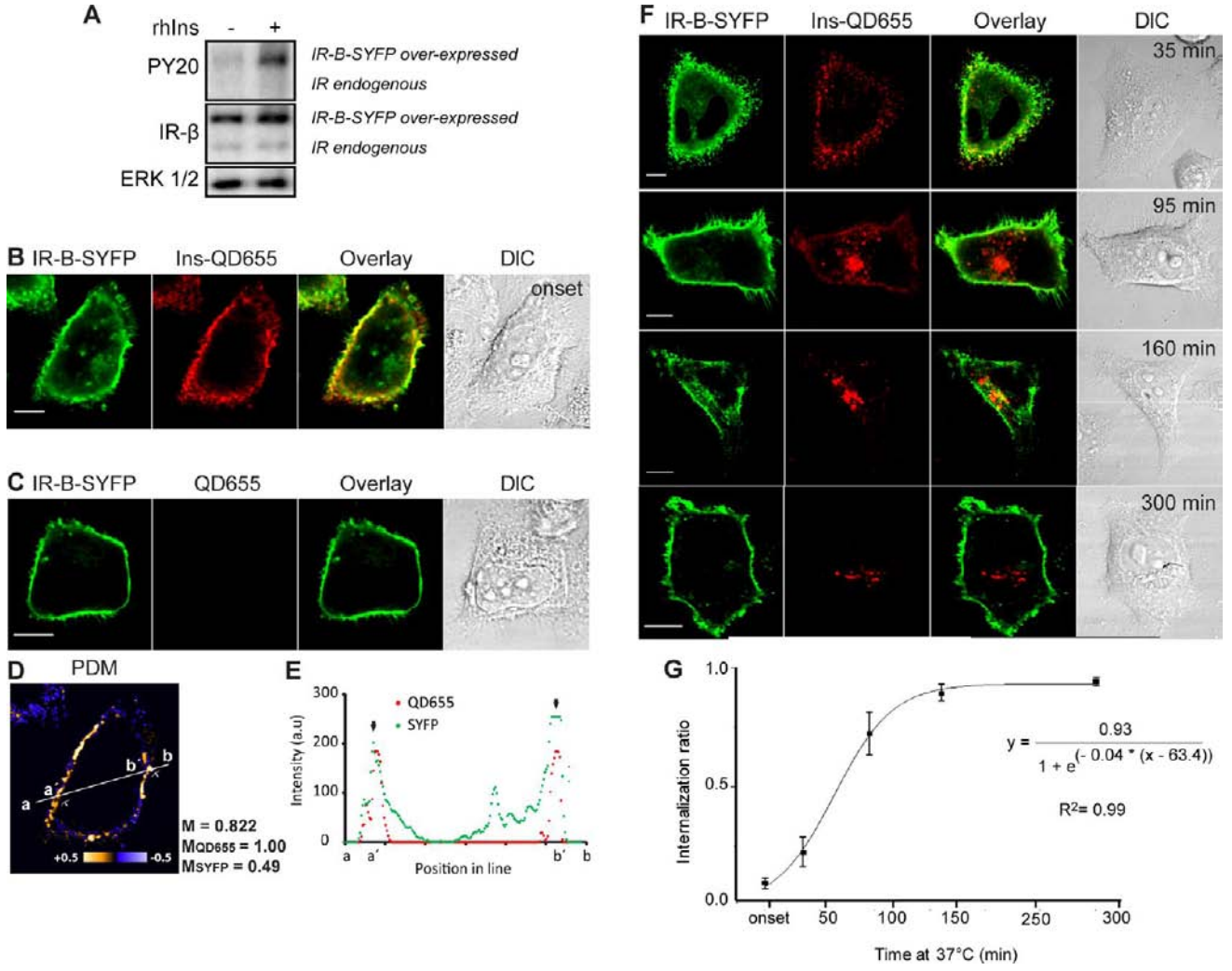

Figure 5. Kinetics of internalization of human insulin in living cells. A. HeLa cells transiently expressing IR-B-SYFP were starved overnight and either not stimulated or stimulated with 100 nM rhIns for 10 min at 37 °C. Lysates were assayed by Western blot. B. Cells expressing IR-B-SYFP labeled with rhIns-PEO_4-biot and QD655 were visualized in vivo by confocal microscopy (Olympus Fluoview FV 1000). Scale bar: 10 μm. C. Cells were only treated with QD655 without rhIns-PEO_4-biot. Acquisition parameters were the same than in panel B. Scale bar: 10 μm. D. PDM graph for cell shown in panel B performed with *ImageJ*. E. Linear trajectories crossing the cell of the two signals using *ImageJ*. F. HeLa cells expressing IR-B-SYFP labeled with 50 nM rhIns-PEO_4-biot and 1 nM QD655 were incubated at 37 °C for 35, 95, 160, and 300 min and visualized in living cells at RT by confocal microscopy (Olympus Fluoview FV 1000). Scale bars: 10 μm. G. Quantification of internalization ratio in individual cells is shown as the mean ± s.e.m. (n = 6−7 cells.)

we estimated the expected molecular masses for each modified peptide (Table 2).

In Figure 4A−D, the spectra obtained after the different treatments are shown. The sample without treatment showed a major peak for insulin (m/z = 5805.6 Da) and a minor one of m/z = 6279.9 Da corresponding to monobiotinylated insulin (see predicted molecular masses, experimental peaks, and assignment in Figure 4E). Analysis showed that we did not obtain insulin modified at the amino terminal of A chain: trypsin treatment followed by DTT showed a single peak (m/z = 2400.8 Da) corresponding to A chain + Na^+ (Figure 4D). DTT treatment showed a minor peak of m/z = 3902.1 Da, corresponding to B chain modified with the PEO_4-biotin group (Figure 4B). After both treatments, we observed a peak (m/z = 2485.0 Da) corresponding to unmodified B chain without the C-terminus (GFFYTPKT) (Figure 4D). Altogether, the evidence leads to the conclusion that the PEO_4-biotin group has been introduced at Lys located at position 29 of B chain and that the amino terminal of A chain, which is important for binding to the IR, remained unmodified.[29,30] The yield of the reaction estimated by MALDI-TOF was 15%.

rhIns-PEO_4-biot Binds IR at the Plasma Membrane. HeLa cells were transfected with the plasmid encoding IR-B fused to SYFP (pcDNA3-R-B-SYFP). We evaluated the correct expression of the fusion protein first by Western blot. IR-B-SYFP was correctly expressed exhibiting the correct size of the β subunit of IR fused with SYFP. This band appeared ~25 kDa higher than that the endogenous IR. It was also confirmed that the IR-B-SYFP was activated after stimulation with rhIns (Figure 5A).

After 48 h of expression, cells were labeled with biotinylated rhIns (rhIns-PEO_4-biotin) and subsequently with different streptavidin−QD655 concentrations (0.5, 1.0, 2.0, 3.0, 4.0 nM) as we described above. Binding was quantified by confocal microscopy imaging. Since QD655 binding was shown to be concentration dependent in the range 0.5−3.0 nM, we decided continue to work with 1 nM, a low unsaturated concentration that does not compromise detection, to ensure single

dx.doi.org/10.1021/bc300526d | *Bioconjugate Chem.* 2013, 24, 431−442

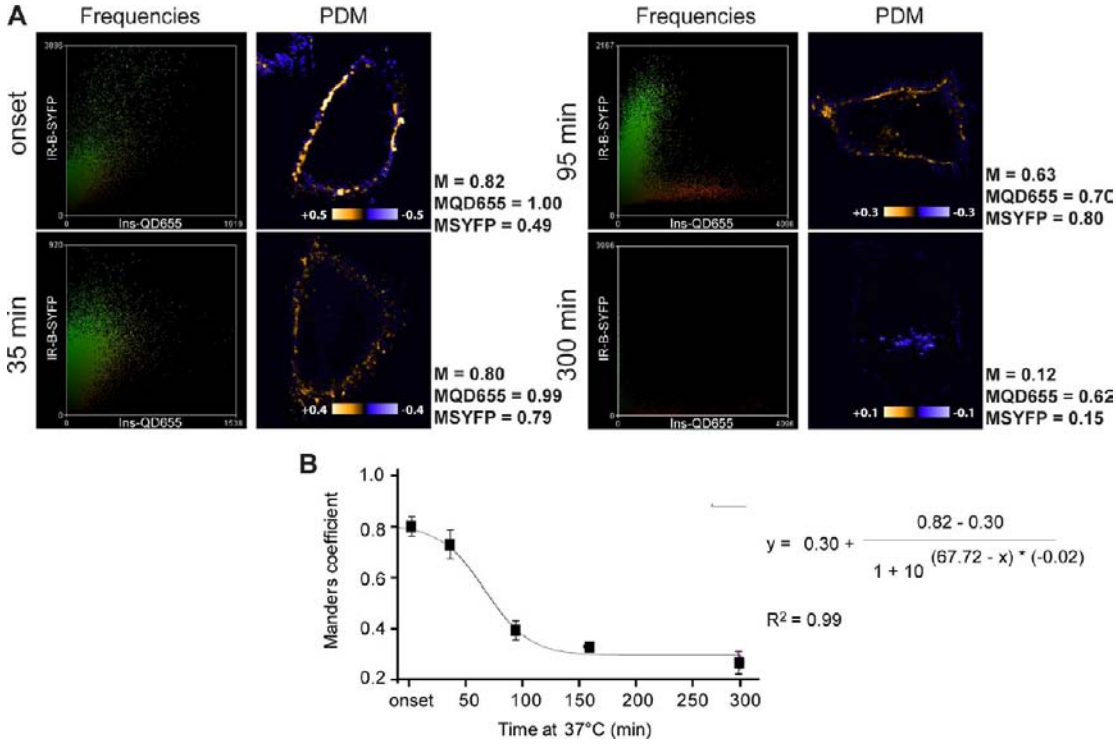

Figure 6. Colocalization of rhIns-QD655 and IR-B-SYFP over the time in vivo. A. Frequencies and PDM graph for cells incubated at 37 °C for 35, 160, and 300 min. IR-B-SYFP signal is the vertical axis and Ins-QD655 the horizontal one in the frequencies plot. *M*: Manders coefficient. M_{QD655}: Manders coefficient in the red channel. M_{SYFP}: Manders coefficient in the green channel. B. Representation of the results performed in individual cells for Manders coefficients. Results are shown as the mean ± s.e.m. (n = 6 cells.)

rhIns-PEO_4-biotin binding to each nanoparticle (data not shown). Only transfected cells showed QD655 labeling, demonstrating that rhIns-PEO_4-biotin was bound to the cells through the IR-B (Figure 5B). Control transfected cells showed no QD655 signal when treated without previous incubation with rhIns-PEO_4-biotin, confirming that QD655 binding was specific (Figure 5C). As expected, whereas SYFP signal was present at the membrane, as well as in the perinuclear region, rhIns-PEO_4-biotin-QD655 was only detected at the membrane.

To analyze the colocalization between IR and its ligand, we calculated Manders coefficients for each cell using the *ImageJ* plugin "Intensity correlation analysis". The PDM (product differences of the mean) graph showed that major contributions to the colocalization coefficient were localized at the plasma membrane (Figure 5D). We also evaluated colocalization across the cell body by superimposing the two signals over a linear trajectory (Figure 5E). The intracellular intensity of SYFP was considerable, reflecting receptor processing in the biosynthetic pathway.

Real Time Imaging of Human Insulin Internalization through IR-B. We next addressed whether modified insulin was capable of being internalized through the IR. Experiments were performed by incubating the cells at 37 °C for different times (35, 95, and 160 min) before imaging by confocal microscopy. Whereas at the onset (no incubation at 37 °C) QD655 signal was localized exclusively at the plasma membrane, after incubation at 37 °C, QDs was detected inside the cell. The fraction of intracellular QD655 increased over time, leading to an accumulation of the signal in perinuclear regions (Figure 5F). To quantify these observations, we performed a segmentation of the cell images into total and interior compartments, and determined the total QD655 signal in both regions. The degree of internalization was obtained from the ratio $QD_{interior}/QD_{total}$ (Figure 5G): 0.09 ± 0.02 (onset); 0.22 ± 0.06 (35 min); 0.72 ± 0.09 (95 min); 0.89 ± 0.03 (160 min); and 0.94 ± 0.02 (300 min) (n = 6–7 cells for each time point). The data were fit to a sigmoid curve (R^2 = 0.99) and calculation of the first derivative was taken as a measure of the internalization rate constant (k), the maximal value of which was 0.009 ± 0.001 min^{-1}.

Endosomal Insulin-IR-B Complex Lifetime. It is generally proposed that IR endocytosis is crucial for turning off the metabolic signaling at the membrane and that signals from the endosomes preferentially target the mitogenic cascade. Thus, internalization on the activated receptor appears to be critical for maintaining signaling balance. We hypothesize that IR remain active in endosomes as long as insulin remains bound to it, and thus determined the kinetics of colocalization as a measurement of insulin–IR complex integrity inside the cell.

Confocal images obtained showed that QD and SYFP signals colocalized at the plasma membrane at the onset of the experiments. This condition was maintained in early endosomal compartments after endocytosis, whereas at latter times, QD signal associated with insulin was distributed in a distinct manner from that of the SYFP (receptor signal) and was probably accumulated in lysosomes (Figure 6A, last panel).

We quantified these observations by calculating Manders coefficients in individual cells for each time point, and generated PDM and frequency plots (Figure 6A). PDM showed differences between the early internalization steps (onset and 35 min) and the late ones (95 and 300 min). At the beginning and up to 35 min, the QD and SYFP frequencies mapped to a line close to 45°; in contrast, after 95 and 300 min the plot showed two populations of pixels for each signal (Figure 6A). Accordingly, colocalization coefficients decreased significantly (p < 0.0001) over time: 0.81 ± 0.02 (onset); 0.74 ± 0.06 (35 min); 0.41 ± 0.04 (95 min);

dx.doi.org/10.1021/bc300526d | *Bioconjugate Chem.* 2013, 24, 431–442

0.34 ± 0.02 (160 min); and 0.28 ± 0.02 (300 min) (n = 6 cells for each time point) (Figure 6B). From this analysis, it was possible to estimate the maximum ligand−receptor dissociation rate: k_{max} = (0.006 ± 0.001) min^{-1}. In addition, we calculated the half-time of colocalization in endocytosed vesicles of 68 min and estimated that after 115 min the degree of colocalization in endocytosed vesicles was reduced by more than 90%. We interpret this value as a characterized dissociation time of the intracellular pool of ligand−receptor complexes, and that mitogenic signaling terminated during the ensuing process of receptor dephosphorylation.

DISCUSSION

In order to study the endocytosis of insulin-IR complexes in living cells, we used biotinylated rhIns conjugated with streptavidin−QD. As compare with conventional fluorescent ligands (FITC-Ins), fluorescent nanoparticles have a high brilliance and stability allowing long-term experiments. In addition, they are photostable and are not affected by pH changes during trafficking and can be combined with different VFPs. To achieve this, we covalently modified rhIns using a biotin bound to a linker constituted by four PEO groups. Reaction product contained unmodified insulin and mono-biotinylated insulin (15%), allowing the imaging of receptor−ligand complex using streptavidin−QDs. Human recombinant biotinylated insulin bound properly to IR and led to its internalization. Between the hormone and the biotin, we introduced a linker of ∼18 Å corresponding to PEO groups. The presence of the linker allowed insulin binding to the IR while conjugated with the nanoparticle.

Biotinylation of human insulin was used in the past to purify the IR by avidin−Sepharose affinity chromatography.[31−34] In order to be used as bifunctional ligands for affinity chromatography of the receptor, insulin analogues should bind simultaneously to avidins and the receptor and bonds must be stable to resist exhaustive washing procedures to remove contaminants from affinity columns. The cited publications addressed two issues: (i) finding a spacer arm long enough to separate the biotin group from insulin active site so that receptor and avidin binding can occur simultaneously; and (ii) selecting chemical reaction conditions avoiding modification of amino terminal of A chain. In our work, we improved both conditions in order to generate labeled insulin allowing imaging of binding and internalization of insulin−IR complex in living cells.

Conjugation of modified human insulin with streptavidin−QD combined the established mode of chemical insulin modification with new nanotechnology for studying IR dynamics and allowed quantification of internalization and dissociation kinetics of insulin−receptor complexes. Although biotinylated insulin, BAC-Ins, and FITC-Ins are commercially available and were successfully applied in cellular studies by microscopy,[35−39] they are of bovine or porcine origin. Here, we applied the modification of rhIns to study the kinetics of the ligand receptor endocytosis and dissociation in a completely human context. In the 1980s and 1990s, numerous papers were published measuring internalization kinetics of IR using traditional radioactive experiments and insulins of different animal origins.[40−43] Some of these reports are discordant, depending on the cells used or the method of analysis. For example, while Draznin and colleagues[39] reported k = 0.049 min^{-1} and a half-time of 14.5 min in rat-isolated hepatocytes using pork radiolabeled insulin, Knuston [42] derived k = 0.0023 min^{-1} and a half-time of 4.9 h using embryonic Swiss mouse fibroblastic 3T3-C2 cells and bovine radiolabeled insulin. In the present work, using HeLa cells, we calculated k = 0.009 min^{-1} and a half-time of 79 min using the human IR-B and human insulin. The methods employed allowed determination of the endocytosis rate constant at later times than those available using radiolabeled ligands.

Internalization of insulin−IR constitutes the major mechanism of insulin degradation and down-regulation of cell surface receptors.[43,44] However, signal transduction by IR is not limited to its activation at the plasma membrane. The activated ligand−receptor complex internalized into endosomes would activate substrates that are spatially distinct from those accessible at the plasma membrane. IR internalization is required for the activation of SHC/MAPK pathway but not for IRS-1 and Akt phosphorylation, suggesting that the latter molecules are activated by IR at the membrane. From this information and the data reported here, we infer that the dynamics of the activated IR depends on the cellular context and it is crucial for the correct balance of its signaling.

It has been postulated that the balance between the metabolic and mitogenic cascade activation depends on the degree of kinase activation.[45,46] Insulin analogues with slower dissociation constants induce a greater degree of mitogenic compared to metabolic signaling than unmodified insulin.[46−48] Moreover, different reports demonstrated a blockage of mitogenic pathway by internalization inhibition.[49−51] Combined internalization and colocalization experiments allowed a comparative and quantitative analysis of dynamics of IR signaling and its termination. We propose that internalization of activated receptor plays a crucial role in the signaling balance. On one hand, it would turn off metabolic signaling by displacing IR from the effector molecules localized at the membrane; on the other hand, mitogenic signaling would be promoted from endosomes, although endosomal trafficking would finally lead to dissociation of insulin−receptor complexes in late endosomes and lysosomes switching off the signaling pathways.

ASSOCIATED CONTENT

Supporting Information

Figure S1 and Figure S2. This material is available free of charge via the Internet at http://pubs.acs.org.

AUTHOR INFORMATION

Corresponding Author

*E-mail: federico@fbmc.fcen.uba.ar. Tel.: (5411) 4576-3300.

Present Address

[‖]Department of Pathology and Immunology, Baylor College of Medicine, One Baylor Plaza, Houston, TX 77030, United States.

Author Contributions

J.G., E.A.J.E., and F.C.L. conceived and designed the experiments; J.G. performed the experiments; J.G., E.A.J.E., and F.C.L. analyzed the data; J.G. and F.C.L.wrote the paper.

Notes

The authors declare no competing financial interest.

[⊥]Deceased on September 29, 2011.

ACKNOWLEDGMENTS

Elizabeth A. Jares-Erijman died during manuscript preparation and we dedicate it to her memory. We thank Laboratorios BETA (Argentina) for providing the rhIns and Dr. M. Cristina Matulewickz (FCEN, UBA) for her help with sample lyophilization. We especially thank Dr. Thomas Jovin for his help and support and Dr. Silvia Moreno for her kindly help

with MALDI-TOF analysis, interpretation, and conclusions. We also thank Dr. Anabella Srebrow for pCMV-Akt-HA plasmid and Dr. Patricia Cuasnicu for anti-PY20 antibody. This work was supported by Max-Planck Society (E.A.J.E., Partner Group grant), University of Buenos Aires (X106), CONICET (Argentina), and ANPCyT (PICT-2006-01365) (Argentina). J.G. was a recipient of a CONICET fellowship and was awarded a short-term EMBO fellowship.

■ ABBREVIATIONS

BAC-Ins, Biotin amido caproyl insulin; BP, band-pass; DCC, *N*,*N*′-dicyclohexylcarbodiimide; DMF, dimethylformamide; DTT, dithiothreitol; EGF, epidermal growth factor; EV, empty vector; FBS, fetal bovine serum; FITC-Ins, Insulin conjugated with FITC; GFP, enhanced green fluorescent protein; GLUT4, glucose transporter 4; HA, human influenza hemagglutinin; IGF, insulin like growth factor; IGF-IR, IGF-I receptor; IR, insulin receptor; IR-B, insulin receptor isoform B; IRS, insulin receptor substrates; M, Manders coefficient; MALDI, matrix-assisted laser desorption/ionization; MAPK, mitogen-activated protein kinase; NHS, *N*-hydroxysuccinimide; PDM, differences from the mean; PEO, polyethylene oxide; PFA, paraformaldehyde; QD, quantum dot; rhIns, recombinant human insulin; RT, room temperature; SCFP, super cyan fluorescent protein; SYFP, super yellow fluorescent protein; TEA, triethylamine; TOF, time-of-flight; VFP, visible fluorescent protein.

■ REFERENCES

(1) Kaplan, S. A. (1984) The insulin receptor. *J. Pediatr. 104*, 327−336.

(2) Belfiore, A., Frasca, F., Pandini, G., Sciacca, L., and Vigneri, R. (2009) Insulin receptor isoforms and Insulin receptor/Insulin-like growth factor receptor hybrids in physiology and disease. *Endocrine Reviews 30*, 1−38.

(3) Bevan, P. (2001) Insulin signaling. *J. Cell Sci. 114*, 1429−1430.

(4) Kouhara, H., Hadari, Y. R., Spivak-Kroizman, T., Schilling, J., Bar-Sagi, D., Lax, I., and Schlessinger, J. (1997) A lipid-anchored Grb2-binding protein that links FGF-receptor activation to the Ras/MAPK signaling pathway. *Cell 89*, 693−702.

(5) Gotoh, N., Toyoda, M., and Shibuya, M. (1997) Tyr phosphorylation sites at amino acids 239 and 240 of Shc are involved in epidermal growth factor-induced mitogenic signaling that is distinct from Ras/mitogen-activated protein kinase activation. *Mol. Cell. Biol. 17*, 1824−1831.

(6) Weng, L. P., Smith, W. M., Brown, J. L., and Eng, C. (2001) PTEN inhibits insulin-stimulated MEK/MAPK activation and cell growth by blocking IRS-1 phosphorylation and IRS-1/Grb-2/Sos complex formation in a breast cancer model. *Hum. Mol. Genet. 10*, 605−616.

(7) Biedi, C., Panetta, D., Segat, D., Cordera, R., and Maggi, D. (2003) Specificity of insulin-like growth factor I and insulin on Shc phosphorylation and Grb2 recruitment in caveolae. *Endocrinology 144*, 5497−5503.

(8) Giudice, J., Barcos, L. S., Guaimas, F., Penas, A., Giordano, L., Jares-Erijman, E. A., and Coluccio Leskow, F. (2012) Insulin and insulin like growth factor II endocytosis and signaling via insulin receptor B. *Cell Communication and Signaling,*.

(9) Di Guglielmo, G. M., Baass, P. C., Ou, W. J., Posner, B. I., and Bergeron, J. J. (1994) Compartmentalization of SHC, GRB2 and mSOS, and hyperphosphorylation of Raf-1 by EGF but not insulin in liver parenchyma. *EMBO J. 13*, 4269−4277.

(10) Bergeron, J. J., Di Guglielmo, G. M., Baass, P. C., Authier, F., and Posner, B. I. (1995) Endosomes, receptor Tyr kinase internalization and signal transduction. *Biosci. Rep. 15*, 411−418.

(11) Grimes, M. L., Zhou, J., Beattie, E. C., Yuen, E. C., Hall, D. E., Valletta, J. S., Topp, K. S., LaVail, J. H., Bunnett, N. W., and Mobley, W. C. (1996) Endocytosis of activated TrkA: Evidence that nerve growth factor induces formation of signaling endosomes. *J. Neurosci. 16*, 7950−7964.

(12) Pol, A., Calvo, M., and Enrich, C. (1998) Isolated endosomes from quiescent rat liver contain the signal transduction machinery. Differential distribution of activated Raf-1 and Mek in the endocytic compartment. *FEBS Lett. 441*, 34−38.

(13) Rizzo, M. A., Shome, K., Watkins, S. C., and Romero, G. (2000) The recruitment of Raf-1 to membranes is mediated by direct interaction with phosphatidic acid and is independent of association with Ras. *J. Biol. Chem. 275*, 23911−23918.

(14) Sorkin, A., McClure, M., Huang, F., and Carter, R. (2000) Interaction of EGF receptor and grb2 in living cells visualized by fluorescence resonance energy transfer (FRET) microscopy. *Curr. Biol. 10*, 1395−1398.

(15) Jensen, M., and De Meyts, P. (2009) Molecular mechanisms of differential intracellular signaling from the insulin receptor. *Vitamins and Hormones 80*, 51−75.

(16) Jares-Erijman, E. A., and Jovin, T. M. (2003) FRET imaging. *Nat. Biotechnol. 21*, 1387−1395.

(17) George, N., Pick, H., Vogel, H., Johnsson, N., and Johnsson, K. J. (2004) Specific labeling of cell surface proteins with chemically diverse compounds. *J. Am. Chem. Soc. 126*, 8896−8897.

(18) Marks, K., and Nolan, G. (2006) Chemical labeling strategies for cell biology. *Nat. Methods 3*, 591−596.

(19) Lidke, D. S., Nagy, P., Heintzmann, R., Arndt-Jovin, D. J., Post, J., Grecco, H. E., Jares-Erijman, E. A., and Jovin, T. M. (2004) Quantum dot ligands reveal EGFR dynamics in living cells. *Nat. Biotechnol. 22*, 198−203.

(20) Lidke, D. S., Lidke, K., Rieger, B., Jovin, T. M., and Arndt-Jovin, D. J. (2005) Reaching out for signals: filopodia sense EGF and respond by directed retrograde transport of activated receptors. *J. Cell Biol. 170*, 619−626.

(21) Lidke, D. S., Nagy, P., Heintzmann, R., Jovin, T. M., and Arndt-Jovin, D. J. (2007) Biotin-ligand complexes with streptavidin quantum dots for in vivo cell labeling of membrane receptors. *Methods Mol. Biol. 374*, 69−80.

(22) Cambi, A., Lidke, D. S., Arndt-Jovin, D. J., Figdor, C. G., and Jovin, T. M. (2007) Ligand-conjugated quantum dots monitor antigen uptake and processing by dendritic cells. *Nano Lett. 7*, 970−977.

(23) Echarte, M. M., Bruno, L., Arndt-Jovin, D. J., Jovin, T. M., and Pietrasanta, L. I. (2007) Quantitative single particle tracking of NGF-receptor complexes: transport is bidirectional but biased by longer retrograde run lengths. *FEBS Lett. 581*, 2905−29013.

(24) Andrews, N. L., Pfeiffer, J. R., Martinez, A. M., Haaland, D. M., Davis, R. W., Kawakami, T., Oliver, J. M., Wilson, B. S., and Lidke, D. S. (2009) Small, mobile Fc epsilon RI receptor aggregates are signaling competent. *Immunity 31*, 469−479.

(25) Sigot, V., Arndt-Jovin, D. J., and Jovin, T. M. (2010) Targeted cellular delivery of quantum dots loaded on and in biotinylated liposomes. *Bioconjugate Chem. 21*, 1465−1472.

(26) Kantelhardt, S., Caarls, W., de Vries, A. H. V., Hagen, G. M., Jovin, T. M., and Arndt-Jovin, D. J. (2010) Specific visualization of glioma cells in living low-grade tumor tissue. *Plos One 5*, e11323 DOI: 10.1371/journal.pone.0011323.

(27) Jensen, P. E., and Wilkinson, K. D. (1989) Probing the structure of processed antigen by using biotin and avidin. Mhc-dependent inhibition of responses to selected biotinyl-insulin derivatives. *J. Immunol. 143*, 3423−3429.

(28) Tsai, Y. J., Rottero, A., Chow, D. D., Hwang, K. J., Lee, V. H. L., Zhu, G., and Chan, K. K. (1997) Synthesis and purification of NB1-palmitoyl insulin. *J. Pharm. Sci. 86*, 1264−1268.

(29) Pullen, R. A., Lindsay, D. G., Wood, S. P., Tickle, I. J., Blundell, T. L., Wollmer, A., Krail, G., Brandenburg, D., Zahn, H., Gliemann, J., and Gammeltoft, S. (1976) Receptor binding region of insulin. *Nature 259*, 369−373.

(30) Markussen, J., Halstrom, J., Wiberg, F. C., and Schäffer, L. (1991) Immobilized insulin for high capacity affinity chromatography of insulin receptors. *J. Biol. Chem. 266*, 18814−18818.
(31) Hofmann, K., Finn, F. M., Friesen, H. J., Diaconescu, C., and Zahn, H. (1977) Biotinyl insulins as potential tools for receptor studies. *Proc. Natl. Acad. Sci. U.S.A. 74*, 2697−2700.
(32) Hofmann, K., Titus, G., Montibeller, J. A., and Finn, F. M. (1982) Avidin binding of carboxyl-substituted biotin and analogues. *Biochemistry 21*, 978−984.
(33) Hofmann, K., Zhang, W. J., Romovacek, H., Finn, F. M., Bothner-By, A. A., and Mishra, P. K. (1984) Syntheses of biotinylated and dethiobiotinylated insulins. *Biochemistry 23*, 2547−2553.
(34) Finn, F. M., Titus, G., and Hofmann, K. (1984) Ligands for insulin receptor isolation. *Biochemistry 23*, 2554−2558.
(35) Hofert, J. F., Mahowald, T. N., Mahowald, N. A., and Heidrick, M. L. (1988) The binding of FITC-insulin to ANAE-positive cells in rat thymus. *Experientia 44*, 37−38.
(36) Ziegler, O., Cantin, C., Germain, L., Dupuis, M., Sekaly, R. P., Drouin, P., and Chiasson, J. L. (1994) Insulin binding to human cultured lymphocytes measured by flow cytometry using three ligands. *Cytometry 16*, 339−345.
(37) Rajagopal, J., Anderson, W. J., Kume, S., Martinez, O. I., and Melton, D. A. (2003) Insulin staining of ES cell progeny from insulin uptake. *Science 299*, 363.
(38) Luo, Y., Xu, H., Huang, K., Zhang, Z., Luo, Q., and Liu, Q. (2005) Imaging on the binding of FITC-insulin with insulin receptors in cortical neurons of rat. *Conf. Proc. IEEE Eng. Med. Biol. Soc. 6*, 5706−5708.
(39) Wang, H., Liu, Z. H., Li, G., and Barrett, E. J. (2006) The vascular endothelial cell mediates insulin transport into skeletal muscle. *Am. J. Physiol. Endocrinol. Metab. 291*, E323−E332.
(40) Draznin, B., Trowbridge, M., and Ferguson, L. (1984) Quantitative studies of the rate of insulin internalization in isolated rat hepatocytes. *Biochem. J. 218*, 307−312.
(41) Hachiya, H. L., Takayama, S., White, M. F., and King, G. L. (1987) Regulation of insulin receptor internalization in vascular endothelial cells by insulin and phorbol ester. *J. Biol. Chem. 262*, 6417−6424.
(42) Knutson, V. P. (1992) Ligand-independent internalization and recycling of the insulin receptor. Effects of chronic treatment of 3T3-C2 fibroblasts with insulin and dexamethasone. *J. Biol. Chem. 267*, 931−937.
(43) Formisano, P., Najjar, S. M., Gross, C. N., Philippe, N., Oriente, F., Kern-Buell, C. L., Accili, D., and Gorden, P. (1995) Receptor-mediated internalization of insulin. Potential role of pp120/HA4, a substrate of the insulin receptor kinase. *J. Biol. Chem. 270*, 24073−24077.
(44) Yamada, K., Carpentier, J. L., Cheatam, B., Goncalves, E., Shoelson, S. E., and Kahn, C. R. (1995) Role of the transmembrane domain and flanking amino acids in internalization and down-regulation of the insulin receptor. *J. Biol. Chem. 270*, 3115−3122.
(45) Wilden, P. A., Backer, J. M., Kahn, C. R., Cahill, D. A., Schroeder, G. J., and White, M. F. (1990) The insulin receptor with phenylalanine replacing Tyr-1146 provides evidence for separate signals regulating cellular metabolism and growth. *Proc. Natl. Acad. Sci. U.S.A. 87*, 3358−3362.
(46) Wilden, P. A., Siddle, K., Haring, E., Backer, J. M., White, M. F., and Kahn, C. R. (1992) The role of insulin receptor kinase domain auto-phosphorylation in receptor-mediated activities. Analysis with insulin and antireceptor antibodies. *J. Biol. Chem. 267*, 13719−13727.
(47) Hansen, B. F., Danielsen, G. M., Drejer, K., Sørensen, A. R., Wiberg, F. C., Klein, H. H., and Lundemose, A. G. (1996) Sustained signaling from the insulin receptor after stimulation with insulin analogues exhibiting increased mitogenic potency. *Biochem. J. 315* (Pt1), 271−279.
(48) Jensen, M., Hansen, B., De Meyts, P., Schäffer, L., and Ursø, B. (2007) Activation of the insulin receptor by insulin and a synthetic peptide leads to divergent metabolic and mitogenic signaling and responses. *J. Biol. Chem. 282*, 35179−35186.
(49) Biener, Y., Feinstein, R., Mayak, M., Kaburagi, Y., Kadowaki, T., and Zick, Y. (1996) Annexin II is a novel player in insulin signal transduction. Possible association between annexin II phosphorylation and insulin receptor internalization. *J. Biol. Chem. 271*, 29489−29496.
(50) Ceresa, B. P., Kao, A. W., Santeler, S. R., and Pessin, J. E. (1998) Inhibition of clathrin mediated endocytosis selectively attenuates specific insulin receptor signal transduction pathways. *Mol. Cell. Biol. 18*, 3862−3870.
(51) Hamer, I., Foti, M., Emkey, R., Cordier-Bussat, M., Philippe, J., De Meyts, P., Maeder, C., Kahn, C. R., and Carpentier, J. L. (2002) An arginine to cysteine (252) mutation in insulin receptors from a patient with severe insulin resistance inhibits receptor internalization but preserves signaling events. *Diabetologia 45*, 657−667.